Coordination Chemistry Reviews 255 (2011) 1104–1116

Contents lists available at ScienceDirect

Coordination Chemistry Reviews

journal homepage: www.elsevier.com/locate/ccr

Review

Structural aspects of mononuclear Mo/W-enzymes

Holger Dobbek*

Institut für Biologie, Strukturbiologie/Biochemie, Humboldt-Universität zu Berlin, Unter den Linden 6, D-10099 Berlin, Germany

Contents

ARTICLE INFO

Article history:
Available online 18 November 2010

Keywords:
X-ray crystallography
Pyranopterin cofactor
Enzyme structure
Molybdoproteins
Hydroxylases

ABSTRACT

This review provides an overview of the contributions of protein X-ray crystallography to the field of pyranopterin-containing W/Mo-enzymes. Several crystal structures for all of the four different families of pyranopterin-containing enzymes have been determined in recent years allowing one to compare overall folds and active site architectures. Especially within the dimethylsulfoxide reductase family and the Mo-containing hydroxylases a diversity of Mo/W-ligands has been discovered, challenging the earlier proposed functions of individual active site components. Reinterpretations of structures and the use of enzyme variants and complexes with inhibitors and slow substrate provided further insights, which will be discussed for the individual enzymes.

1. Introduction

The determination of protein structures and their active site architectures contributed extensively to our knowledge about the mechanism of enzymes using the pyranopterin cofactor to coor-

* Tel.: +49 30 20936369; fax: +49 30 20936447.
E-mail address: holger.dobbek@biologie.hu-berlin.de

0010-8545/$ – see front matter © 2010 Elsevier B.V. All rights reserved.
doi:10.1016/j.ccr.2010.11.017

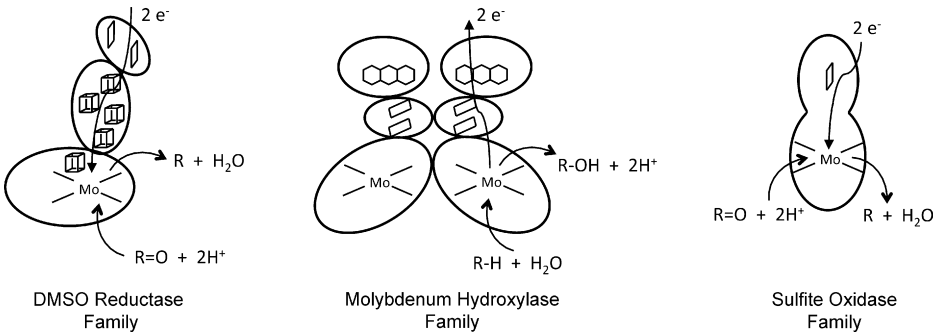

Fig. 1. Three families of Mo-pyranopterin containing enzymes. Schematic representation of the prototypical composition of enzymes in the DMSO reductase, molybdenum hydroxylase and sulfite oxidase family. Please note that while only one direction for each reaction is indicated, both reactions are catalyzed depending on enzyme and substrate.

dinate molybdenum and tungsten. This review attempts to give an overview on the currently available structures of pyranopterin-cofactor containing enzymes.

At the time of writing this review 111 coordinate entries in the protein data bank (PDB) belong to Mo- or W-bound pyranopterin-containing enzymes, which are derived from the crystal structure analysis of 19 enzymes with different catalytic activities. While in a review written 2001 it was still possible to present images of the overall structures of all pyranopterin-containing enzymes of known structure at that date [1], the number of structures in the database makes this approach impossible in 2010 and illustrative examples have to be chosen for in-depth discussions. Several reviews on the structure of pyranopterin-containing enzymes have appeared within the last years and are suggested as complementary reading [2–4].

Enzymes containing the pyranopterin cofactor may be divided into four families, which share similar amino acid sequences, core structure surrounding the pyranopterin cofactor(s) and have a common theme in the coordination of their central Mo/W ion (Figs. 1 and 2) (for general reviews on pyranopterin-containing enzymes see: [5–7]). The pyranopterin cofactors interact with the protein matrix by hydrogen-bonds and coordinate the Mo/W ion through their dithiolene group. Different coordination geometries for the Mo ion within enzymes have been described, however all geometries may be unified when the dithiolene group of the pyranopterin cofactor is treated as a single bidentate ligand straddling over one vertex of a tetrahedron, allowing one to describe all geometries as more or less distorted tetrahedra (Fig. 2) [1,8].

2. Enzymes of the DMSO reductase family

The largest family of molybdoproteins is formed by enzymes related to dimethylsulfoxide (DMSO) reductase. These enzymes occur in bacteria and archaea, catalyze proper oxygen-atom-transfer (OAT) reactions and contain two pyranopterin cofactors to coordinate the central Mo-ion (Fig. 2). Despite some sequence and structural similarities, the family diverges in terms of overall size, number of subunits and cofactor composition (Supplementary Table). All enzymes share similar core structures consisting of four conserved α/β domains grouped around the *bis*-pyranopterin guanosine dinucleotide (*bis*-PGD) cofactor, a fold first encountered in the crystal structure of DMSO reductase from *Rhodobacter sphaeroides* [9] (Fig. 3). A classification scheme dividing the enzymes of the DMSO reductase family into three subfamilies [10], will be used to discuss related enzymes in the following sections.

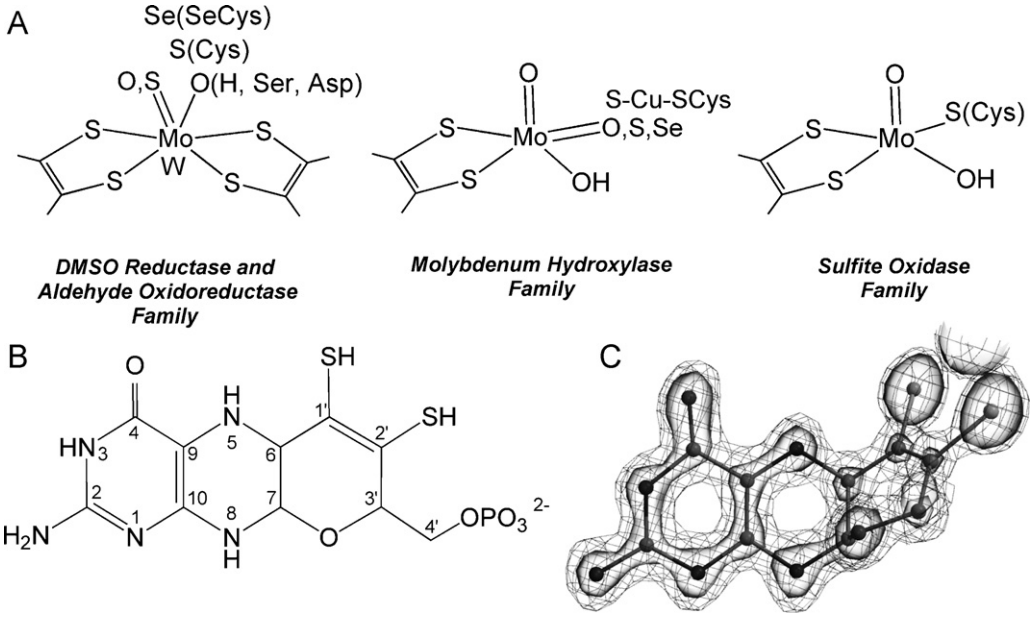

Fig. 2. The pyranopterin cofactor. (A) Active site architectures of the four families of pyranopterin-containing enzymes. The DMSO reductase family and the tungsten-containing aldehyde oxidoreductase family contain both *bis*-pyranopterin containing enzymes and are depicted by the same picture. (B) The pyranopterin-cofactor without metal bound. Coordination of molybdenum and tungsten occurs through the dithiolene group at the pyran ring. (C) Structure of the pyranopterin-cofactor with a $2F_{obs} - F_{calc}$ electron density map at two different contour levels.

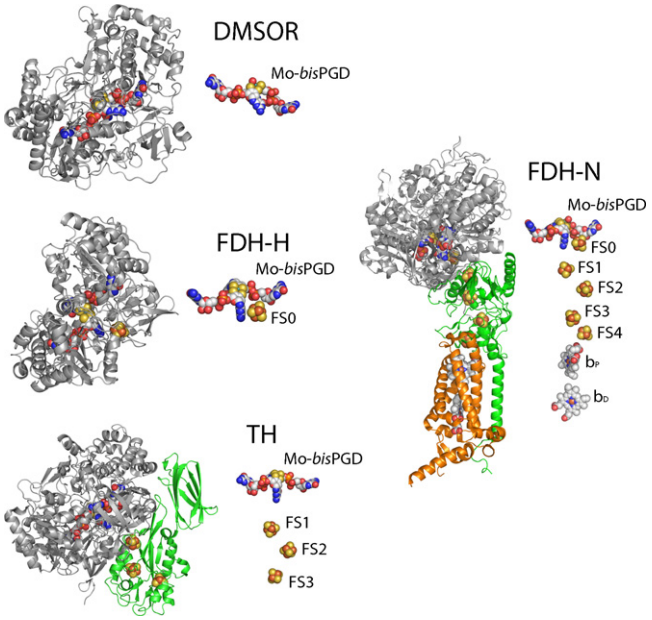

Fig. 3. DMSO reductase family: Subunit structure and cofactors. DMSOR: Structure of the DMSO reductase from *R. capsulatus*. FDH-H: Structure of the formate dehydrogenase H from *E. coli*. TH: Structure of the pyrogallol:phoroglucinol transhydroxylase from *Pelobacter acidigallici*. FDH-N: Structure of formate dehydrogenase H from *E. coli*. Iron–sulfur clusters are labeled with FS and numbered, the two heme-groups labeled b_P and b_D for proximal and distal *b*-type heme, are part of the membrane bound subunit of FDH-N. The Mo-subunits are colored in white, the iron–sulfur containing subunits in green and the heme-containing subunit in orange. All cofactors are shown as spheres with elements colored white for carbon, blue for nitrogen, yellow for sulfur, red for oxygen and orange for phosphor. All figure have been prepared using PyMol [140]. (For interpretation of the references to color in text, the reader is referred to the web version of the article.)

2.1. Formate dehydrogenases

Formate dehydrogenases (FDHs) are atypical members of the DMSO reductase family as they do not catalyze a formal OAT, but the reversible oxidation of formate to carbon dioxide, two electrons and a proton [11]. The interconversion of carbon dioxide and formate is central to the one-carbon metabolism of several bacteria and archaea, and occurs as an intermediate step in energy conserving pathways [12].

The first structure of a FDH to be determined was that of the *Escherichia coli* enzyme FDH-H, a component of the anaerobic formate hydrogen lyase complex. The crystal structure of FDH-H was also the first structure of a molybdoenzyme containing a selenocysteine, revealing more about the function of the 21st amino acid in catalysis [13]. The highly dioxygen sensitive enzyme was produced, purified and crystallized under strictly anoxic conditions to prevent contact with air at any stage of preparation [14,15]. In addition to a Mo-ion coordinated by the *bis*-PGD cofactor, the structure of FDH-H resolved the position of a [4Fe–4S]-cluster, which is close to the pterin portion of one of the two *bis*-PGDs (Fig. 3). The protein was crystallized in the oxidized and formate reduced state and the structures revealed a larger movement of one PGD cofactor upon oxidation of Mo [15]. Selenocysteine had originally been modeled as a ligand of Mo in the reduced (Mo(+IV)) and oxidized (Mo(+VI)) state of the enzyme. However, in a recent paper the original diffraction data were subjected to new refinement programs and a careful analysis revealed selenocysteine to be no longer bound to Mo in the formate-reduced state, but displaced by 9 Å from its original position [16], in agreement with EXAFS studies of the enzyme [17]. This suggested new roles of the selenocysteine in the reaction, which may be able to form a selenium-carboxylated intermediate [18], and may explain why its exchange against cysteine results in a 300-fold reduced activity [19,20]. The re-interpretation of the data further indicated the terminal Mo-ligand to be a sulfido and not a hydroxo/oxo ligand as originally modeled.

The structure of a far more complex FDH from *E. coli* (FDH-N) was revealed in 2002 [21]. FDH-N is a membrane-bound protein and its expression is induced in the presence of nitrate in the growth medium. Special care had to be taken to solubilize FDH-N and to separate it from the membrane-bound nitrate reductase [22]. Despite the large size of the protein, crystals diffracted to 1.6 Å resolution, allowing the careful placement and analysis of all cofactors, making it one of the best-resolved membrane protein structures. With 11 redox centers (Supplementary Table) including the Mo-site, five [4Fe–4S]-cluster, two *b*-type heme groups and a bound menaquinone analog, the structure of FDH-N became a model for

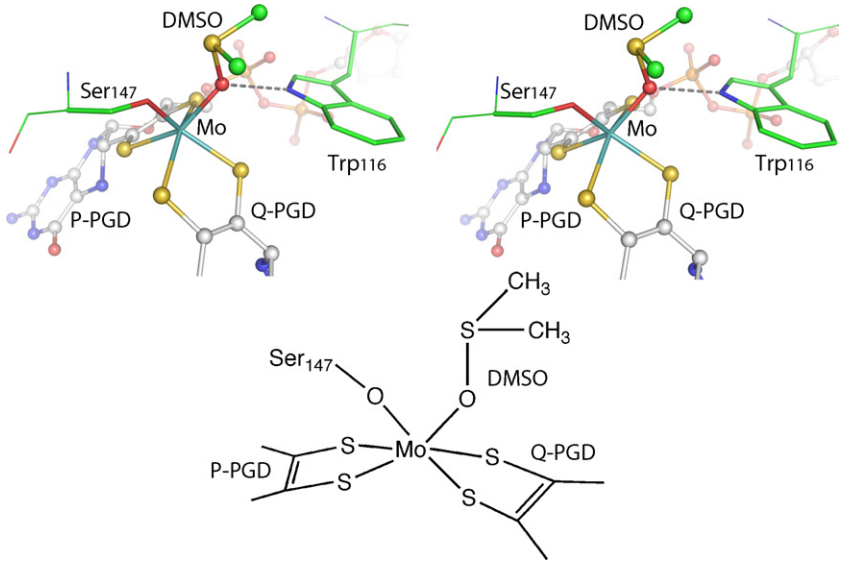

Fig. 4. Stereoview on the active site of DMSO reductase with bound DMSO. Coordinates have been taken from PDB-Id: 4DMR [56]. The substrate DMSO is bound *via* its oxygen atom to Mo, which is in hydrogen-bonding distance and geometry to the indole ring of Trp116. Ser147 is a ligand of Mo in all states of DMSO reductase so far examined. The second oxo-ligand at Mo present in the coordinates is not shown as it has a strong overlap of van-der-Waals radii with neighboring atoms and has been assigned to a density peak likely originating from an alternative position displaying the non-physiological pentacoordinate Mo [51]. The Mo-bound *bis*-PGD cofactor (labeled as Q-PGD and P-PGD) and the substrate are shown as balls and sticks, while the amino acids are shown as sticks only.

the more complex members of the DMSO reductase family (Fig. 4). The tight packing of three heterotrimeric monomers with extensive interfaces suggests a physiological $(\alpha\beta\gamma)_3$ arrangement of FDH-N in the membrane. Three subunits harbor the cofactors and position them in a chain within the typical distances of 8–12 Å [23] spanning altogether a distance of 90 Å and 340 V in potential difference between formate oxidation at Mo and reduction of menaquinone in the membrane portion [21]. A complex redox chain with several cofactors, predominantly iron–sulfur cluster, is also found in other metalloenzymes as in hydrogenase [24], fumarate reductase [25,26] and complex-I of the respiratory chain [27–29]. The structure of FDH-N was resolved in the oxidized state and like in the soluble FDH-H selenocysteine is found as a Mo-ligand. The α-subunit is larger than in FDH-H, but has a very similar core structure including conserved positions for Mo *bis*-PGD and one [4Fe–4S]-cluster. The structure provides direct insights into the likely mechanism of energy conservation in a redox loop [30] between FDH-N and nitrate reductase to generate a proton-motive force on the cytoplasmatic membrane.

A less complex but tungsten-containing FDH can be found in the sulfate reducing bacterium *Desulfovibrio gigas* [31]. Despite its different metal contents the structure is overall similar to FDH-N, including fold, composition and Mo/W-coordination, in which again selenocysteine acts as a ligand [32,33]. The small subunit is similar to the β-subunit of FDH-N, but lacks one [4Fe–4S]-cluster.

2.2. Nitrate and polysulfide reductases

Nitrate reductases catalyze the reduction of nitrate with two electrons and two protons to nitrite and water [11,34]. Different types of Mo-containing nitrate reductases are found in eukaryotic and prokaryotic organisms, and the former will be discussed together with the related sulfite oxidases. Prokaryotic nitrate reductases exist as simple enzymes of a single subunit similar in structure to FDH-H as well as complex membrane-bound enzymes similar to FDH-N.

The structure of the soluble periplasmatic dissimilatory nitrate reductase isolated from *Desulfovibrio desulfuricans* was reported at a resolution of 1.9 Å [35]. The enzyme was crystallized in the oxidized state and is similar to FDH-H, with a cysteine instead of the selenocysteine residue acting as protein ligand to Mo. A closer relationship between the two enzymes is also indicated by the side reactivities of both enzymes, which can catalyze the reaction of the other enzyme with low activity. The earlier interpretation of an oxo-ligand bound to Mo was revised when the long Mo-ligand distance and the low B-factor of the ligand were noticed [36]. By comparing the anomalous scattering properties of O and S it was observed that the terminal Mo-ligand cannot be derived from water but should contain sulfur. This also explains the unusual short distance of 2.2 Å between the former oxo-ligand and the thiolate of the Mo-coordinating cysteine (PDB-Id: 2NAP), which can now be attributed to the partial formation of a disulfide-bond. The reinterpretation of the structure stimulates a revision of the proposed mechanisms and the non-innocence (participation of the ligands in the redox chemistry) [37] of the S-ligand has been proposed and may also be relevant for FDH [36,38].

Additional complexity of the electron transfer chain in nitrate reductases was resolved by the structural and kinetic work of Arnoux et al. [39], who studied NapAB from *Rhodobacter capsulatus*. The complex between NapA, the molybdoprotein, and NapB, a diheme *c*-type cytochrome, can only form after transport into the periplasm due to the two different transport pathways used in the maturation of both proteins. Complex formation changes the structure and also the redox potential of the [4Fe–4S]-cluster in NapA [39].

Structurally more complex than the soluble nitrate reductases are the membrane-bound enzymes belonging to subfamily II of the DMSO reductase family. The membrane-bound nitrate reductase complex from *E. coli* is composed of NarG (molybdoprotein), NarH (polyferredoxin) and NarI (*b*-type cytochrome), which form a $(\alpha\beta\gamma)_2$ oligomer. The structure of NarGHI was resolved for the oxidized enzyme at a resolution of 1.9 Å [40]. Similar to membrane-bound FDH-N, NarGHI consists of a large extra membranous part covering NarGH and the membrane anchored *b*-type diheme cytochrome NarI. The cofactors comprise a *bis*-PGD bound Mo, two *b*-type heme groups and five iron–sulfur clusters, one of which is a [3Fe–4S]-cluster. One of the [4Fe–4S]-clusters has the more unusual 3xCys, 1xHis coordination and gives rise to a high-spin ($S = 3/2$) signal [41]. The structure of NarGHI further revealed one PGD cofactor in the usual tricyclic (pyranopterin) and one in the unusual bicyclic (pterin) state with open pyran ring, as proposed to occur before the first structures of Mo-enzymes were elucidated [42]. Based on this observation it was suggested that scission and condensation of the pyran-ring may participate in the catalytic proton transfer reaction. Mo is coordinated by the carboxylate of aspartate in a bidentate fashion, adding aspartate and its carboxylate group as new members to the list of protein ligands of Mo in the DMSOR family (Fig. 2). Furthermore, the structure of NarGH, a shorter version of the NarGHI complex in which the membrane anchor is missing, was elucidated [43]. While the overall structure is similar, Asp here acts as a monodentate ligand and an oxo-ligand completes the hexacoordinated Mo sphere. However, the short distance of 1.6 Å between the oxo-ligand and the coordinating carboxylate oxygen of aspartate, as well as the 2.3–2.4 Å distance between the oxo-ligand and one dithiolene-sulfur create an overlap of the respective van-der-Waals radii and indicates some structural heterogeneity (PDB-Id: 1R27).

Similar to NarGHI, polysulfide reductase is an integral membrane protein coupling the reduction of polysulfides to the oxidation of menahydroquinone-7 at a similar Mo-site as in nitrate reductase [44]. The structure of the polysulfide reductase revealed a novel type of membrane-anchor architecture, which is indicative of a proton-pumping scheme using conformational changes [44].

2.3. Ethylbenzene dehydrogenase

Ethylbenzene dehydrogenase catalyzes the hydroxylation of ethylbenzene to 1-(*S*)-phenylethanol, the first step in the anaerobic degradation of aromatic hydrocarbons by *Aromatoleum aromaticum* [45]. The crystal structure at 1.88 Å resolution revealed a complex metalloenzyme with striking similarities to NarGHI, although the protein is soluble and not membrane-bound like NarGHI [46]. Ethylbenzene dehydrogenase consists of three different subunits, contains one pyranopterin with a closed and one with an open pyran ring coordinating the Mo and features an aspartate as protein ligand at Mo. An acetate molecule completes the coordination of Mo. It shares with NarGHI the presence of a His-coordinated [4Fe–4S]-cluster and has an unprecedented Met–Lys coordination of the *b*-type heme group.

The reaction of ethylbenzene dehydrogenase is unusual in that it hydroxylates a rather inert hydrocarbon instead of the usually found polar substrates. The mechanism was suggested to proceed through radical intermediates to a carbocation on the substrate, which becomes hydroxylated by the Mo(IV)-H_2O species formed [47,48].

2.4. Dimethylsulfoxide reductases

DMSO reductases catalyze the reversible reduction of DMSO with two electrons and two protons to dimethylsulfide (DMS). The first structure of a member of the DMSO reductase family was pub-

lished in 1996 [9] and revealed the first *bis*-PGD coordinated Mo ion. The structure of DMSO reductase is of special interest as the enzyme was intensely investigated by spectroscopic methods and specifically the lack of additional cofactors in the enzyme facilitated the use of UV/Vis absorption spectroscopy to follow the reaction at the Mo site, whose absorption is usually covered by the more intensively absorbing iron–sulfur clusters, heme groups or flavins. Shortly after the structure of the DMSO reductase isolated from *R. sphaeroides* was published a second DMSO reductase structure emerged, this time from an enzyme isolated from the closely related organism *R. capsulatus* [49]. Consistent with the high amino acid sequence identity both structures were overall very similar but revealed different coordinations for the Mo ion. That these variations were not species dependent, but reflected the variability of the Mo-coordination was demonstrated when a third DMSO reductase structure, again from enzyme isolated from *R. capsulatus*, with another variation in the active site structure was presented [50]. A high-resolution structure from the *R. sphaeroides* enzyme brought the likely explanation and resolved a mixture of a hexacoordinate and a pentacoordinate Mo-ion, which appear to be present in the other structures with variable populations [51]. In the hexacoordinate structure Mo is coordinated by the four sulfurs of *bis*-PGD, the side chain of serine and an oxo-ligand (Figs. 2 and 4). This structure is transformed into the pentacoordinate structure by dissociation of one PGD from Mo, which is replaced by a second oxo-ligand. While the hexacoordinated structure is consistent with extended X-ray absorption spectroscopy (EXAFS) data [52,53] and most likely represents the oxidized state of the active species, the pentacoordinate structure likely represents an inactive state of DMSO reductase [54,55]. A structure with DMSO in the active site revealed the substrate to be directly bound to Mo *via* its oxygen atom and is in agreement with the Mo–OH being the oxygen source [56] (Fig. 4). In contrast to other enzymes in which the addition of tungsten instead of molybdenum to the bacterial growth medium results in pyranopterin-deficient enzymes, tungsten can be incorporated into DMSO reductase in place of Mo. The coordination geometry is very similar compared to the Mo-containing enzyme but W-DMSO reductase is more active in DMSO reduction but has a strongly impaired DMS oxidation activity [57], likely reflecting the lower oxidation potential of the W(+VI)/W(+IV) couple compared to the Mo couple.

2.5. Pyrogallol-phloroglucinol transhydroxylase and acetylene dehydratase—the non-redox enzymes

Pyrogallol-phloroglucinol transhydroxylase catalyzes an overall non-redox reaction consisting of a reductive dehydroxylation and an oxidative hydroxylation as two consecutive steps. The Mo-coordination is closely related to that of DMSO reductase (Supplementary Table) and like DMSO the substrate pyrogallol coordinates the Mo-ion directly [58]. The architecture of the active site supports a mechanism in which both substrate and cosubstrate bind simultaneously in the active site [59]. Despite the non-redox reaction catalyzed transhydroxylase contains three [4Fe–4S]-cluster bound to its β-subunit. As electron uptake/donation does not play a role in the catalyzed reaction, it is suggested that the iron–sulfur clusters may be evolutionary remnants from an ancestral redox enzyme.

Another non-redox reaction, the hydration of acetylene to acetaldehyde, is catalyzed by the oxygen-sensitive W-containing enzyme acetylene hydratase. The structure provides evidence for a new type of substrate channel guiding acetylene to a different portion of the W-coordination when compared to the related Mo-containing nitrate reductase [60]. Acetylene hydratase is active in the reduced (W(+IV)) state in which H_2O coordinates the W-ion. Substrate docking calculations indicate the binding of acetylene directly above the W-bound water ligand. The role of W(+IV) is to activate the water ligand, which would act as an electrophile attacking the triple bond of acetylene to form a vinyl cation intermediate. The structure-based mechanism thus avoids a W-bound acetylene complex suggested by computational investigations of the mechanism [61].

2.6. Arsenite oxidase

Arsenite oxidase catalyzes the oxidation of arsenite to arsenate and is unique among the members of the DMSO reductase family in its cofactor content and molybdenum coordination [62]. In the structure Mo is pentacoordinate with the dithiolene-groups of the *bis*-PGD and an oxo-ligand [63]. In contrast to other members of the DMSO reductase family it does not involve a protein ligand to coordinate the Mo. The enzyme was crystallized in the oxidized state but most likely became photoreduced during data collection. In agreement with EXAFS data the authors thus argue that the pentacoordinate form is likely representing the reduced state and a hexacoordinated state with one oxo- and one hydroxo-ligand is likely to be found in the oxidized state. Arsenite oxidase is the only Mo-enzyme of known structure harboring a Rieske-[2Fe–2S] cluster, which is typically employed for electron transfers at more positive reduction potentials than the *all*-Cys coordinated iron–sulfur cluster.

3. Molybdenum hydroxylases

Molybdenum hydroxylases catalyze reactions following the general scheme $R\text{–}H + H_2O \rightarrow ROH + 2e^- + 2H^+$. In contrast to monooxygenases, which also catalyze hydroxylation reactions, the source for the hydroxyl-group incorporated into the substrate is water and not dioxygen, and redox equivalents are generated and not consumed [64,65]. Compared to the DMSO reductase family the molybdenum hydroxylase family is more homogenous in its cofactor composition and active site architecture (Supplementary Table). Two classes may be defined consisting of the molybdo-iron–sulfur proteins and the molybdo-iron–sulfur flavoproteins, with the latter being more abundant (Fig. 5). The active site architectures of all characterized members are similar and consist of oxo/hydroxo-, sulfido-, selenido-ligands occurring, with the exception of the enzyme carbon monoxide dehydrogenase, as terminal ligands of Mo (Fig. 6). The characteristic essential terminal sulfido-ligand at Mo had been used in the pre-genome sequence area to identify members of the molybdenum hydroxylases and its nature and function has been regarded as key to the reactivity of the enzymes [8]. The sulfido ligand reacts with cyanide to thiocyanate, producing the inactive Mo tri-oxo state of the enzymes [66–69]. The catalytic relevance of the sulfido ligand may be explained from the electronic structure of the *cis*-MoOS unit in which a highly delocalized Mo=S π^* LUMO acts as an electron sink in orbital-controlled reactions [70]. However, it was recently demonstrated that at least one molybdenum hydroxylase, the aldehyde oxidoreductase isolated from *D. gigas*, is active in the Mo tri-oxo state (Fig. 6-I) [71].

3.1. Xanthine oxidoreductases

Xanthine oxidoreductases (XORs) have been isolated from a wide range of organisms and catalyze the hydroxylation of a variety of purines, pyrimidines, pterins and aldehydes. The physiological function of mammalian XORs is to act in the last steps of the degradation of purines to urate *via* hydroxylation of hypoxanthine to xanthine. The mammalian enzyme is synthesized in the xanthine dehydrogenase form, which may be converted by oxidation of sulfhydryl groups or proteolysis to the oxidase form. XORs are large homodimeric enzymes with a mass of about 290 kDa. Each

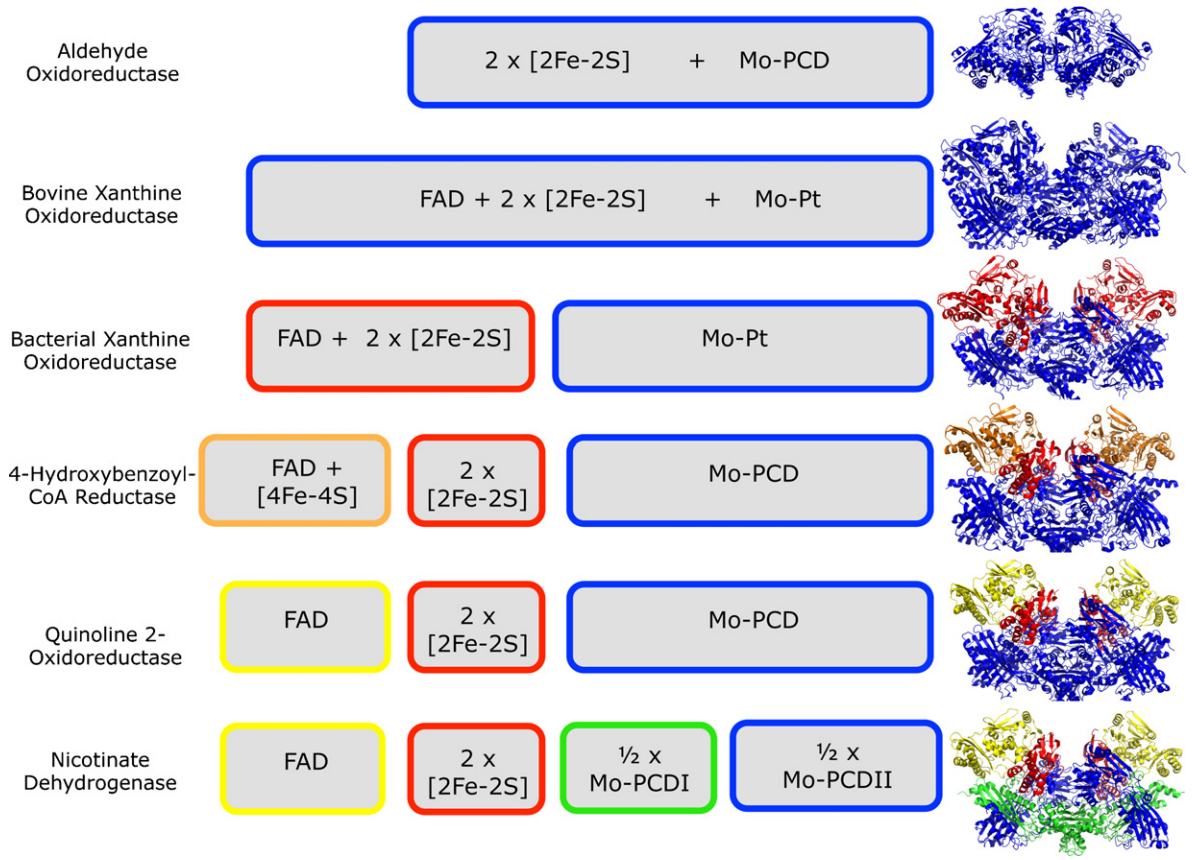

Fig. 5. Composition of Mo-hydroxylases. Subunits and their cofactors are listed in the boxes and the ribbon presentation next to it has the same color code as the frames of the boxes. Mo-PCD denotes the Mo-bound form of the pyranopterin-cytosine-dinucleotide cofactor, while Mo–Pt stands for the Mo-bound pyranopterin cofactor.

monomer contains the pyranopterin cofactor, two [2Fe–2S]-cluster and FAD, which is the prototypical cofactor content for molybdenum hydroxylases.

Enroth et al. resolved the structure of the bovine xanthine dehydrogenase (XDH) form at 2.1 Å and the xanthine oxidase (XO) form at 2.5 Å [72,73]. Mild proteolytic digestion resulted in three fragments separating the molybdenum containing domain, the iron–sulfur cluster domain and the FAD-domain. Distances of 12–14 Å between the four cofactors are in agreement with a through-space electron transfer from Mo to FAD [23]. The resolution of 2.1 Å did not allow to unambiguously identify the nature of the three terminal ligands of Mo, which were inferred from the arrangement found in the structure of (re)sulfurated aldehyde oxidoreductase from *D. gigas*, where the crucial sulfido-ligand was localized in the apical position [74]. The protein was cocrystallized in the presence of salicylate to protect the active site, and a salicylate molecule was found in the structure to block the substrate channel. Electron paramagnetic resonance (EPR) spectroscopy has been used to differentiate the two [2Fe–2S]-cluster, designated as type-I and type-II [75,76]. Two different domains bind the two [2Fe–2S]-cluster; one domain resembles a plant-type [2Fe–2S]-cluster ferredoxin and carries the type-II [2Fe–2S]-cluster, the fold

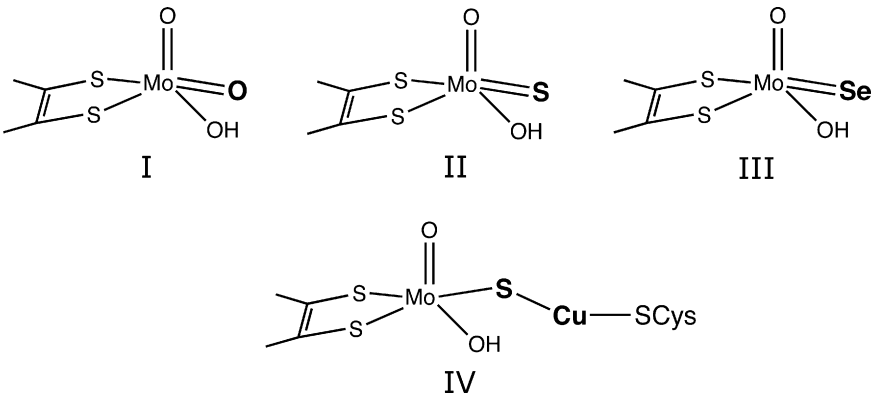

Fig. 6. Active sites of Mo-hydroxylases. Four variations in the active site of Mo hydroxylases have been found. (I) The [MoO_3] species is found in the inactive states of CODH, XOR and quinoline 2-oxidoreductase and represents the active form of the aldehyde oxidoreductase from *D. gigas* [71]. (II) The [$MoSO_2$] unit is the active state of most molybdenum hydroxylases and contains the cyanolyzable sulfido-ligand in the equatorial position. (III) A [$MoSeO_2$] unit has been found in the active site of nicotinate dehydrogenase from *E. barkeri* and is likely present in several molybdenum hydroxylases from *Clostridia*. (IV) The [$CuSMoO_2$] unit is the active site metal cluster of carbon monoxide dehydrogenases.

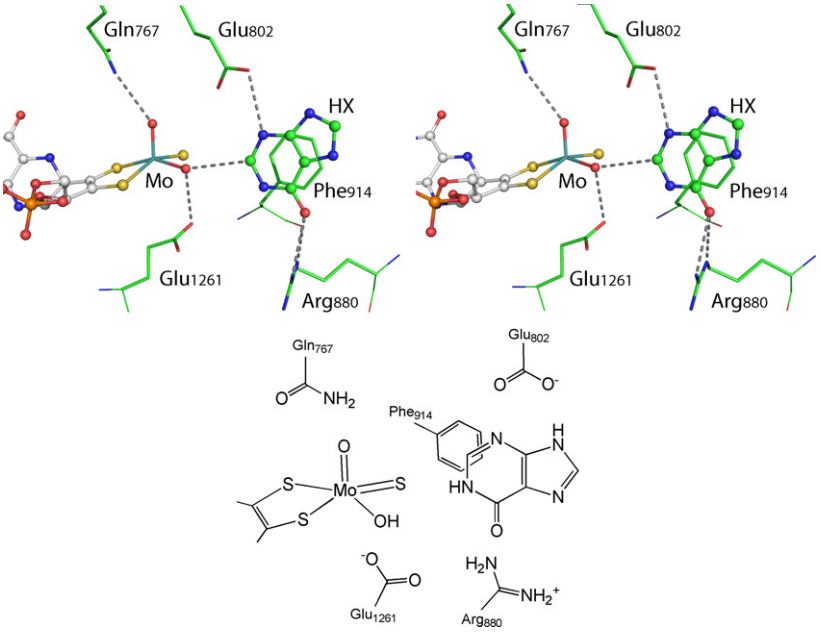

Fig. 7. Stereoview on the active site of bovine xanthine oxidoreductase with bound hypoxanthine. Coordinates have been taken from PDB-Id: 3NRZ [91]. Hypoxanthine is labeled with HX and is positioned with its C2 atom close to the equatorial hydroxo ligand, which is the hydroxylating species. Gln767 is in hydrogen-bonding distance to the apical oxo-ligand, which is supposed to act as a spectator. Glu1261 serves as a catalytic base abstracting a proton from the equatorial hydroxo-ligand, when it reacts with the substrate. Negative charges developing on the substrate during hydroxylation are proposed to be stabilized by Arg880. Glu802 is in hydrogen-bonding distance to the N-3 atom of hypoxanthine. The Mo-bound pyranopterin cofactor and the substrate are shown as balls and sticks while the amino acids are shown as sticks only. All cofactors are shown as spheres with elements colored white for carbon, blue for nitrogen, yellow for sulfur, red for oxygen and orange for phosphor. (For interpretation of the references to color in text, the reader is referred to the web version of the article.)

of the second domain comprises a four-helix bundle and carries the type-I [2Fe–2S]-cluster. The FAD-containing domain may be divided into three subdomains. Two motifs involved in FAD binding, –AAGTP– and –TIGG– are similar to the FAD binding site of flavoenzymes of the vannilyl alcohol oxidase family [77] and the N-terminal and middle subdomains show the core fold typical for this enzyme family [73,78].

Proteolytic cleavage of the surface exposed loops leads to the irreversible XDH-to-XO conversion and partially blocks access of the electron acceptor NAD^+ to $FADH_2$ and changes the electrostatic environment of the flavin site. Both changes account for the switch in substrate specificity from NAD^+ (XDH) to dioxygen (XO) as electron acceptor. Kuwabara et al. identified a cluster of residues that build the center of a relay system for the conversion of XDH to XO and the gating of a solvent channel leading to FAD [79]. The involvement of two cysteine residues (Cys535 and Cys992) in the reversible XDH-XO conversion was later confirmed and refined by studies on mutant XORs [80]. However, also mutations near the flavin site stabilize the XO form [81].

XOR from *R. capsulatus* is similar in sequence to mammalian XOR, but consists of two subunits forming a dimer of heterodimers $(\alpha\beta)_2$ in solution. Specific functional inactivation of one active site per *R. capsulatus* XOR dimers shows that the individual monomers are active and act without cooperative effects within the homodimers [82]. In contrast to the majority of bacterial molybdoenzymes *R. capsulatus* XOR does not contain the dinucleotide form of the pyranopterin and the structure is more closely related to the mammalian XORs than to other bacterial molybdenum hydroxylases like quinoline 2-oxidoreductase. Allopurinol is similar to hypoxanthine, but acts as an inhibitor of XORs and is used as a drug to treat hyperuricemia and to aid in cases of post ischemia reperfusion injury. Cocrystallization of bacterial XOR with allopurinol produced a complex between XOR and the inhibitor tightly bound *via* its N8 atom to Mo. Both, biochemical assays as well as the observed electron density indicate that allopurinol is first hydroxylated before the resulting alloxanthine (also called oxipurinol) binds to Mo(+IV). The same mode of alloxanthine binding has been confirmed at higher resolution for mammalian XOR [83].

Effective inhibitors of XOR are not necessarily chemically/structurally related to (hypo)xanthine. Febuxostat (TEI-6720; 2-(3-cyano-4-isobutoxyphenyl)-4-methyl-5-thiazole carboxylic acid) is a non-purine inhibitor, which binds with a dissociation constant in the low nanomolar to picomolar range to XOR and acts as a mixed-type inhibitor. The crystal structure of the resulting complex revealed it to bind in the substrate channel leading to Mo. TEI-6720 blocks the channel and the immediate environment of Mo, but unlike alloxanthine does not interact with Mo. A similar mode of inhibition has also been found for the related inhibitor Y-700 [84].

An intermediate in the hydroxylation reaction was captured with a slow substrate of XOR and shows the Mo–O–C bond formed [85]. The high-resolution structure also allowed one to define the stereochemistry of the Mo ligands proving that the crucial sulfido-ligand is indeed found in an equatorial position, which is widely conserved in the Mo-hydroxylase family (Fig. 6) [86–88]. In the structure with the slow substrate the sulfido-ligand is most likely protonated and Mo in the reduced state (Mo + IV) [85]. A structure of XOR with a slow purine substrate (2-hydroxy-6-methylpurine) was resolved at 2.3 Å [89]. 2-hydroxy-6-methylpurine is, like xanthine, hydroxylated at C-8. The structure supports the idea that xanthine would bind with the C-6 carbonyl positioned to interact with Arg880 to stabilize the Mo(+V) transition state (Fig. 7). This proposal is further supported by crystal structures of bacterial XOR in complex with hypoxanthine, xanthine and pterin-6-aldehyde, which are all oriented with their C-6 carbonyl towards the conserved Arg (Arg880 in bovine XOR) [90]. A recent high-resolution structure of bovine XOR reveals two orientations for hypoxanthine, one in which C2 of hypoxanthine is close to the hydroxylating Mo-ligand and one in which C8 of hypoxanthine would become hydroxylated [91] (Fig. 7). The latter

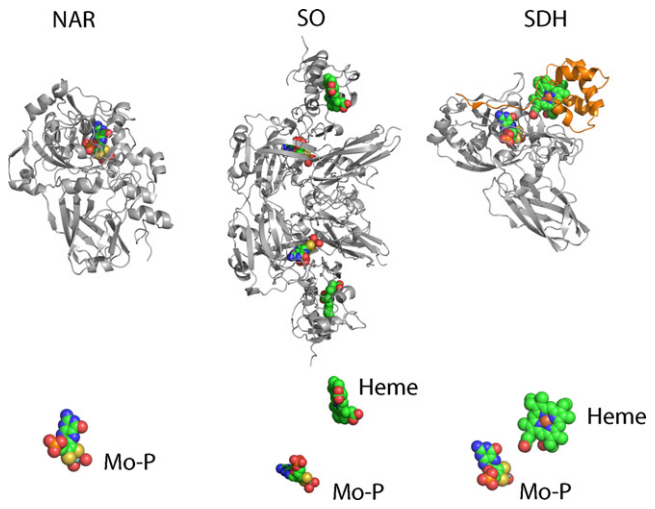

Fig. 8. Architecture of sulfite oxidizing enzymes. NAR: Structure of the assimilatory nitrate reductase from *A. thaliana*. SO: Sulfite oxidase from chicken liver. SDH: Structure of the sulfite dehydrogenase from *Starkeya novella*. The Mo-subunits are colored in white and the heme-containing subunit in orange. All cofactors are shown as spheres with elements colored green for carbon, blue for nitrogen, yellow for sulfur, red for oxygen and orange for phosphor. (For interpretation of the references to color in text, the reader is referred to the web version of the article.)

reaction is suggested to be disfavored by the lower reactivity of the C8 atom.

Recombinant protein expression and site-directed mutagenesis together with X-ray crystallography also allows analyzing the contributions of individual residues to different substrate specificities [92]. In the XOR related mammalian aldehyde oxidase most residues in the active site are conserved, but Glu802 is exchanged for valine and in place of Arg880 a methionine residue is found in sequence alignments. The corresponding mutations in XOR convert it to an aldehyde oxidase-like enzyme, supporting the idea that these residues are instrumental to achieve the various substrate specificities [92].

3.2. Aldehyde oxidoreductases from sulfate-reducing bacteria

Aldehyde oxidoreductases (AORs) from sulfate-reducing bacteria catalyze the oxidation of aldehydes with a wide range of different side groups to carboxylic acids. The crystal structure of AOR from *D. gigas* was the first structure of a Mo-pyranopterin containing enzyme to be determined [93]. Mo is coordinated by the dithiolene moiety of a pyranopterin cytosine dinucleotide (PCD) cofactor and three oxygen containing ligands, later in a high resolution structure (d_{min} = 1.28 Å) defined as two oxo and one water ligand [94]. The cofactors arrangement (PCD and 2 × [2Fe–2S]-cluster) is very similar to XOR, but AOR lacks the flavin domain/subunit (Fig. 4). Incubation of AOR with sulfide resulted in formation of a Mo-bound sulfido-ligand in the apical position, while crystals of AOR isolated under aerobic or anaerobic conditions had no sulfido-ligand [74]. The activity of AOR does not depend on the presence of a sulfido-ligand at Mo explaining the lack of a sulfido-ligand in all as-isolated structures [71]. Isopropanol was used as a precipitating agent in the crystallization drop and is found in the active site near the Mo ion [93]. The dimer arrangement of AOR differs from that found for XOR. However, like in XOR both monomers act independently from each other and active AOR monomers created in reverse micelles are spectroscopically indistinguishable from the homodimer [95].

XOR and AOR are inhibited by the addition of arsenite. The structure of arsenite-inhibited AOR shows that arsenite coordinates Mo *via* an oxygen bridge and binds at the place of the labile hydroxo-/water ligand of Mo [96,97]. Alcohols like ethylene glycol and glycerol bind to reduced AOR and inhibit the enzyme by replacing the catalytically labile hydroxy/water ligand and exhibit a short Mo–C distance [71]. Short Mo–C distances have earlier been proposed to be of catalytic relevance [98,99] and the observation of a Mo–C distance of 2.4 Å in the AOR–ethylene glycol complex was taken as an additional indication that Mo–C bond containing intermediates may be involved in turnover [71]. Short Mo–C distances of 2.5–2.7 Å have been observed in other Mo-containing structures like the n-butylisocyanide complex of CODH [86] and in the active site of nitrate reductase [40], where the short Mo–C distances are the consequence of Mo–O–C–S and Mo–O–C–O metallocycles. These Mo-containing ring structures are likely related to the formaldehyde inhibited state of xanthine oxidoreductase, where recent ENDOR studies could exclude Mo–C bond formation [100] (for a recent review on Mo–C bonds in molybdenum hydroxylases see [101]).

AOR from *D. gigas* and *D. desulfuricans* share 68% sequence identity and their structures can be superimposed with an r.m.s. deviation for the C-α atoms of 0.8 Å [102].

3.3. 4-Hydroxybenzoyl-CoA reductase

4-Hydroxybenzoyl-CoA reductase from *Thauera aromatica* catalyzes a central step in the anaerobic degradation of phenolic compounds. Its activity is unique among the molybdenum hydroxylases in that the enzyme catalyzes the *de*hydroxylation of a phenolic compound [103,104]. Compared to other molybdenum hydroxylases it has an insertion of 41 amino acids in its β-subunit (FAD-subunit) positioning a [4Fe–4S]-cluster in 16 Å distance from the isoalloxazine ring of FAD [105] (Fig. 5). The insertion effectively covers the otherwise largely solvent accessible FAD-binding site. The [4Fe–4S]-cluster is the likely entry point of electrons derived from a ferredoxin in an inverted electron flow to the Mo. The structure shows Mo in the oxidized state, where it is coordinated by the dithiolene group of PCD, two oxo- and one hydroxo-ligand. An additional electron density peak in *trans* to the apical oxo-ligand is lost after treatment with cyanide. Treatment with dithionite inactivates the enzyme by binding to both equatorial coordination sites of Mo [106].

3.4. Quinoline 2-oxidoreductase

Quinoline 2-oxidoreductase catalyzes the first step in the degradation of quinoline along the 8-hydroxycoumarin pathway of *Pseudomonas putida* 86 by hydroxylating quinoline at the C2 atom [107]. The enzyme is a dimer of heterotrimers $(\alpha\beta\gamma)_2$ and contains the PCD to coordinate Mo, whose terminal ligands have been modeled as two oxo- and one sulfido-ligand, with the sulfido-ligand being an equatorial ligand [87]. A mixture between the substrate quinoline and cryoprotectant glycerol was modeled into the electron density of the active site, positioning the C2 carbon of quinoline to be hydroxylated close to the equatorial hydroxo- and sulfido-ligands.

3.5. Nicotinate dehydrogenase

Nicotinate dehydrogenase from *Eubacterium barkeri* catalyzes the hydroxylation of nicotinate to 6-hydroxynicotinate [108]. Its reactivity is dependent on the presence of a labile selenium moiety, which is not present as selenocysteine [109–111] and is close to the Mo active site [112]. Dependence on a non-selenocysteine selenium moiety has been demonstrated for several Mo hydroxylases mostly isolated from anaerobic bacteria of the order *Clostridiales* and is a unique feature of this group of enzymes [113–115]. The crystal

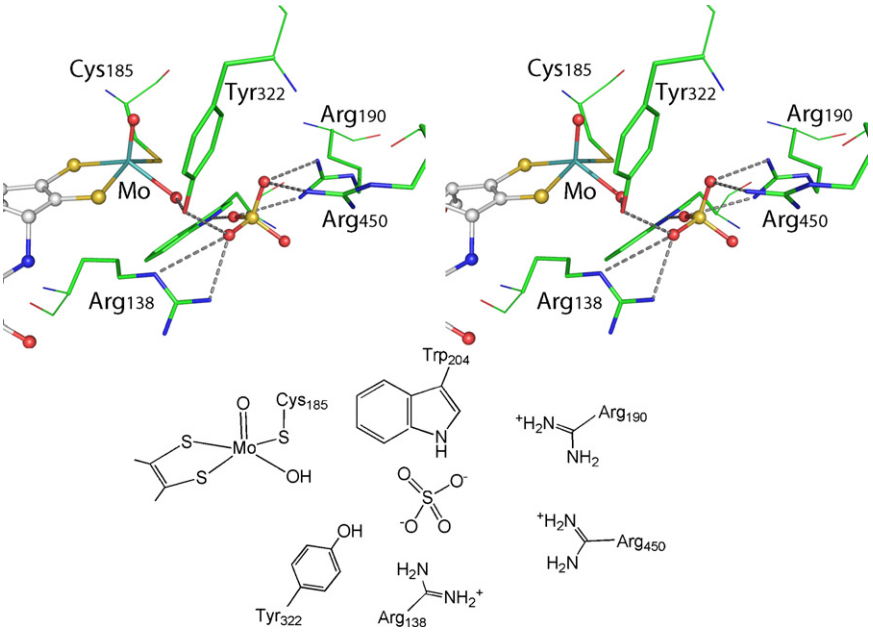

Fig. 9. Stereoview on the active site of sulfite oxidase with bound sulfate. Coordinates have been taken from PDB-Id: 1SOX [121]. A sulfate ion from the crystallization solution has been found in the active site near the Mo-ion and serves as a model for the product bound state of sulfite oxidase. Arginine residues in the active site are positioning the sulfate ion by several salt-bridges and two hydrogen-bond donors (Tyr322, Trp205) further contribute to substrate/product binding. The Mo-bound pyranopterin cofactor and the sulfate ion are shown as balls and sticks, while the amino acids are shown as sticks only.

structure revealed the arrangement of the four subunits as $(\alpha\beta\gamma)_2$ placing all cofactors in a similar position as that seen in carbon monoxide dehydrogenase, XOR and quinoline 2-oxidoreductase (Fig. 5) [88]. Mo is coordinated by PCD and two terminal O- and one terminal Se-ligands. The selenido ligand is found in the position occupied by the cyanolyzable sulfido ligand in other molybdenum hydroxylases and most likely facilitates the formal hydride transfer from the substrate into the low lying π^* orbital of the Mo=Se bond [88,116] (Fig. 6-III).

3.6. Carbon monoxide dehydrogenase

Carbon monoxide dehydrogenases (CODHs) are found in aerobic and anaerobic microorganisms. While anaerobic microorganisms contain mono- and bifunctional Ni,Fe-containing CODHs with a $[NiFe_4S_4OH_x]$-cluster to oxidize CO [117], aerobic carboxydothrophic bacteria like *Oligotropha carboxidovorans* use a Mo-containing enzyme closely related to XORs. Mo–CODHs consist of three different subunits each carrying one type of cofactor [78]. Mo is coordinated by the PCD and was first described as coordinated by three O-containing ligands close to an erroneously interpreted S-selanylcysteine [78]. The crystallographic analysis of a preparation with higher specific activity at true atomic resolution (d_{min} < 1.2 Å) using analytical multiple wavelength anomalous scattering methods revealed a hetero-dinuclear $[CuSMoO_2]$ site, in which the sulfido-ligand of Mo acts as a bridging ligand to a Cu(I) ion with a nearly linear –μS-Cu-SCys– coordination (Fig. 6-IV) [86]. The strong super-hyperfine coupling with $I = 3/2$ nuclear spin of Cu detected in the EPR spectra shows that the electron spin of Mo(V) is efficiently delocalized along the Mo–S–Cu bond [86]. The strong super-hyperfine coupling was also found in a model complex of the active site [118]. Treatment with cyanide inactivates CODH, changes the Mo(V) EPR signal, destroys the dinuclear cluster and results in the formation of a Mo *tri*-oxo species bound in the active site. Treatment of the $[MoO_3]$ species with sulfide and Cu^+ partially restores the $[CuSMoO_2]$ cluster and reactivates the enzyme [119]. A complex of Mo–CODH with n-butylisocyanide, a CO analog, has been resolved at 1.09 Å. The complex reveals the cyano-group inserted between Cu and Mo, with the carbon atom forming a –Mo–O–C–S– metallocycle with a Mo–C distance of 2.6 Å [86].

The Mo–CODH isolated from *Hydrogenophaga pseudoflava* has been structurally characterized with and without bound PCD cofactor and in the latter 5′-cytosine diphosphate (CDP) is found in the place of the CDP moiety of the PCD cofactor [120].

4. Sulfite oxidase family

Sulfite oxidase and assimilatory nitrate reductase are grouped into a separate family of molybdoenzymes. This family originally comprised only enzymes of eukaryotic origin, but recently the structure of two bacterial enzymes, the sulfite dehydrogenase from *Starkeya novella* and the *E. coli* enzyme YedY, showed clear homologies to the eukaryotic proteins and therefore are included in this family of Mo-enzymes.

4.1. Sulfite oxidase and sulfite dehydrogenase

Eukaryotic sulfite oxidases catalyze the oxidation of sulfite to sulfate, the last step in the vital degradation of the sulfur-containing amino acids cysteine and methionine. Sulfite oxidase activity may be lost due to defects in the biosynthesis of the pyranopterin cofactor or due to mutations in the structural gene of the enzyme ("isolated sulfite oxidase deficiency") and may lead to severe neurological abnormalities and mental retardation.

The homodimeric enzyme carries the Mo-pyranopterin and a heme group as cofactors, which are bound in the middle and N-terminal domain of the three-domain protein [121]. The pyranopterin cofactor, one oxo- and one hydroxo-/water-ligand and the thiolate group of a highly conserved cysteine residue coordinate Mo. The *bis*-histidyl coordinated heme-group in the cytochrome b_5-domain is about 32 Å away from Mo and a rearrangement of the flexible domains is necessary to facilitate electron transfer by bringing the two cofactors closer together [122]. A sulfate ion is

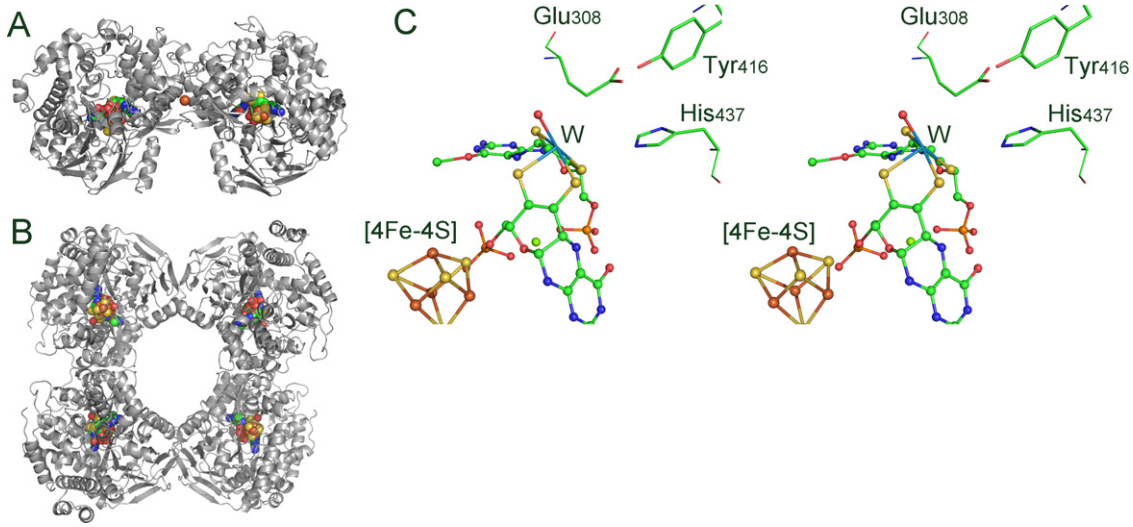

Fig. 10. Overall and active site structure of the W-containing aldehyde ferredoxin oxidoreductase. (A) Overall structure of the aldehyde ferrededoxin oxidoreductase from *Pyrococcus furiosus* (PDB-Id: 1AOR) [134]. (B) Overall structure of the formaldehyde ferredoxin oxidoreductase from *P. furiosus* (PDB-Id: 1B25) [135]. (C) Stereoview on the active site of the formaldehyde oxidoreductase (PDB-Id: 1B25). The protein backbone is shown as white cartoons. All cofactors are shown as spheres with elements colored green for carbon, blue for nitrogen, yellow for sulfur, red for oxygen and orange for phosphor. (For interpretation of the references to color in text, the reader is referred to the web version of the article.)

found in the active site and its position indicates that, like in the molybdenum hydroxylases, the apical oxo-ligand acts as a "spectator" [123], while the equatorial O-ligand is the catalytically labile exchangeable residue [121] (Fig. 9). Mutations affecting sulfite oxidase activity in humans have been localized and two mutations are near the sulfate-binding site, while two other mutations localize near the dimer interface. Recombinant production of chicken liver sulfite oxidase allowed one to study the kinetic and structural alterations of the disease-causing amino acid substitutions directly [124]. Arg450 is critical for catalysis and adopts different conformations in the presence and absence of sulfate in the active site, which are disabled when a neighboring arginine residue is exchanged against glutamine (R138Q) (Fig. 9). Exchange of the Mo-ligating cysteine residue (Cys185) against serine and alanine inactivates the enzyme. The replaced amino acids do not interact with the Mo, where a third oxo-ligand is found in place of the lost Mo–Cys interaction.

A sulfite oxidase from *Arabidopsis thaliana* has been overproduced and crystallized. The plant-type sulfite oxidase is homodimeric and is similar in sequence to mammalian sulfite oxidases, displays a similar fold and Mo coordination. However, plant-type sulfite oxidase lacks the heme-domain and has a different surface charge distribution [125].

Bacterial sulfite dehydrogenases are heterodimeric enzymes. The sulfite dehydrogenase (SorAB) from *S. novella* has been overproduced and its structure solved. SorA binds the Mo-pyranopterin cofactor and SorB is a *c*-type cytochrome (Fig. 8). In contrast to chicken liver sulfite oxidase the distance between the two cofactors is close enough to allow facile electron transfer (Mo-Fe: 16.6 Å; Pyranopterin-Heme: 8.5 Å) [126], Mo-coordination is analogous to chicken liver sulfite oxidase. The short distance between the cofactors and the extensive subunit interface indicate a rigid electron transfer pathway. This is in line with the missing influence of viscosity on the rate of intramolecular electron transfer in bacterial sulfite dehydrogenase [127]. The exchange of an active site Tyr for Phe increased the affinity of the enzyme for dioxygen as electron acceptor and destabilized the conformation of an active site arginine (Arg55) proposed to be involved in substrate binding [128]. Consequently, the substitution R55M increases the apparent K_m for sulfite by 2–3 orders of magnitude [129].

4.2. Nitrate reductase

The assimilatory NAD(P)H:nitrate reductase catalyzes the reduction of nitrate to nitrite with electrons gained from the oxidation of NAD(P)H at a flavin site passing *via* a heme-cofactor. The Mo-containing fragment was crystallized in the presence and absence of sulfate and refined to 1.7 Å resolution (Fig. 8) [130]. The Mo-pyranopterin binding domain is very similar to chicken liver sulfite oxidase and also the Mo coordination (pyranopterin, Cys, one hydroxo, one oxo) is analogous to the related sulfite oxidase, again with clear indications of photoreduction of the crystals by the synchrotron beam.

A structure-based mechanism, which is similar for sulfite oxidase and nitrate reductase, features the direct coordination of nitrate to Mo and an inner-sphere electron transfer to reduce the substrate. Surprisingly, the mechanisms for nitrate reduction in dissimilatory nitrate reductase and the assimilatory nitrate reductase appear to be different.

4.3. YedY

A novel Mo-containing oxidoreductase has been discovered in a screen of the *E. coli* genome sequence for Mo-containing enzymes [131]. The novel protein, YedY, is part of the YedYZ operon encoding a heterodimeric membrane-bound complex, in which YedZ acts as a *b*-type heme containing membrane anchor [132]. The overall fold of YedY and its active site composition is similar to that found in chicken liver sulfite oxidase including the presence of a pyranopterin cofactor. Mo is coordinated by Cys and oxygen-containing ligands. Based on the similarity of the fold YedY has been grouped together with the sulfite oxidase enzymes [133] but its physiological role is likely to be different from the sulfite oxidizing enzymes.

5. Tungsten-containing enzymes of the aldehyde oxidoreductase family

5.1. Aldehyde ferredoxin oxidoreductase

The first enzyme carrying a pyranopterin cofactor, whose structure was elucidated was that of the aldehyde ferredoxin

oxidoreductase (AFOR) from the hyperthermophilic archaeon *Pyrococcus furiosus* [134]. This W-containing enzyme carries two pyranopterin cofactors to coordinate W *via* their dithiolene groups (Fig. 10). The phosphates of the pyranopterin interact with a Mg^{2+} ion, linking both cofactors in a pseudosymmetric protein environment. The active sites in the homodimeric structure are more than 40 Å apart. Each monomer contains one [4Fe–4S]-cluster, with a shortest Mo-Fe distance of 9 Å. In addition to the *bis*-pyranopterin coordination two electron density peaks were observed near W and indicate the presence of two oxo-ligands.

5.2. Formaldehyde ferredoxin oxidoreductase

Formaldehyde ferredoxin oxidoreductase (FFOR) and AFOR share 40% identity in their amino acid sequences and have similarly sized subunits. FFOR forms a stable tetramer with a 222-molecular symmetry [135]. Its active site architecture is similar to AFOR, but also shows parallels to the active site of Mo-containing aldehyde oxidoreductase from *D. gigas* [135], rendering mechanistic similarities possible. A cocrystal structure with the electron transfer partner, a [4Fe–4S]-ferredoxin, shows that the [4Fe–4S]-cluster of FFOR and the ferredoxin are in a short distance forming a pathway for electron transfer from the W-site to the [4Fe–4S]-ferredoxin.

6. Conclusions and outlook

Structures derived from protein crystallography made important contributions to our understanding how Mo-containing enzymes work and will likely continue to do so. However, with the number of enzyme structures rapidly rising new challenges emerge for the future work, which will be briefly outlined below.

X-ray crystallography and its limitations: Due to the size of pyranopterin-containing enzymes X-ray crystallography is the predominant method used to investigate their structures. Protein X-ray crystallography is based on the interaction of X-ray photons with electrons, resulting in coherent scattering used to determine the structure of the electron distribution (electron density). The crystal structure thus does not directly follow from the diffraction experiment, but is derived from the interpretation of the electron density by the crystallographer and the refinement of the model to explain the electron density. While the interpretation may be straightforward when amino acids and cofactors of known composition, for example flavin and heme groups, are concerned, complex metal sites and their inorganic ligands pose a challenge to the crystallographer. Limited resolution originating from weak diffraction, heterogeneity of the metal site(s) and modification of the metal site due to chemistry caused by the photons while the crystal is subject to the X-ray diffraction experiment further obscure the analysis. It is thus not surprising that several structures of metalloenzymes have been revised and others will likely be challenged in the future. High resolution, ideally close to atomic resolution or true atomic resolution (d_{min} < 1.2 Å) is instrumental to resolve mixed states, which otherwise are overlooked, resulting in irrelevant structures. Clearly, the combination of methods, specifically spectroscopic methods sensitive to the oxidation state and geometry of the metal site and the X-ray diffraction experiment are needed to resolve ambiguous cases and first studies of this type have been reported (see for examples: [71,96,97]).

Mechanistic insights from crystal structures: During the last years the aim of many crystallographic studies of metalloenzymes has shifted. While the number of "new" structures deposited per year is not increasing, the crystallographic analysis is more and more often combined with kinetic, spectroscopic and mutagenesis studies and the structure of different enzyme variants, structures with inhibitors and slow substrates give insight into the catalytic cycle. Thus, the structural analysis complements the biochemical work and helps to interpret the result of binding assays and site-directed mutagenesis. On the other hand, crystal structures are the basis for computational studies, which, after years of focusing on the active site metal alone, now include more and more of the surrounding protein matrix (see the accompanying paper by Walter Thiel and Sebastian Metz). A very productive combination appears to lie in the combination of structural methods with kinetic approaches investigating native enzymes and enzyme variants with normal and slow substrates to trap different intermediates along the reaction coordinate. The recent insights into the mechanism of xanthine oxidoreductases obtained in this way are especially encouraging [85,89–91,136,137].

Discovery of novel enzymes: The rapidly rising number of sequenced genomes and the possibility to express pyranopterin-containing enzymes in heterologous expression hosts, makes it likely that soon more Mo-containing enzymes of unknown functions will be studied. This creates new demands and makes the assignment of functions and physiological roles a predominant task for scientists interested in Mo-containing enzymes. It is very likely that protein X-ray crystallography in combination with *in silico* docking studies and enzyme assays will be able to aid the functional assignment of novel pyranopterin-containing enzymes, as demonstrated recently for another class of enzymes [138,139].

Acknowledgements

Work on pyranopterin-containing enzymes in my laboratory has been supported by the Deutsche Forschungsgemeinschaft (DFG DO 785/2) and FCI, which are gratefully acknowledged. I further thank Dr. Berta MDP Martins for critical reading of the manuscript.

Appendix A. Supplementary data

Supplementary data associated with this article can be found, in the online version, at doi:10.1016/j.ccr.2010.11.017.

References

[1] H. Dobbek, R. Huber, Met. Ions Biol. Syst. 39 (2002) 227.
[2] M.J. Romao, J. Knablein, R. Huber, J.J. Moura, Prog. Biophys. Mol. Biol. 68 (1997) 121.
[3] C. Kisker, H. Schindelin, D.C. Rees, Annu. Rev. Biochem. 66 (1997) 233.
[4] M.J. Romao, Dalton Trans. 21 (2009) 4053.
[5] R. Hille, Chem. Rev. 96 (1996) 2757.
[6] M.K. Johnson, D.C. Rees, M.W. Adams, Chem. Rev. 96 (1996) 2817.
[7] G. Schwarz, R.R. Mendel, M.W. Ribbe, Nature 460 (2009) 839.
[8] C.G. Young, J. Biol. Inorg. Chem. 2 (1997) 810.
[9] H. Schindelin, C. Kisker, J. Hilton, K.V. Rajagopalan, D.C. Rees, Science 272 (1996) 1615.
[10] C.A. McDevitt, P. Hugenholtz, G.R. Hanson, A.G. McEwan, Mol. Microbiol. 44 (2002) 1575.
[11] J.J. Moura, C.D. Brondino, J. Trincao, M.J. Romao, J. Biol. Inorg. Chem. 9 (2004) 791.
[12] J.G. Ferry, FEMS Microbiol. Rev. 7 (1990) 377.
[13] A. Bock, K. Forchhammer, J. Heider, W. Leinfelder, G. Sawers, B. Veprek, F. Zinoni, Mol. Microbiol. 5 (1991) 515.
[14] V.N. Gladyshev, J.C. Boyington, S.V. Khangulov, D.A. Grahame, T.C. Stadtman, P.D. Sun, J. Biol. Chem. 271 (1996) 8095.
[15] J.C. Boyington, V.N. Gladyshev, S.V. Khangulov, T.C. Stadtman, P.D. Sun, Science 275 (1997) 1305.
[16] H.C. Raaijmakers, M.J. Romao, J. Biol. Inorg. Chem. 11 (2006) 849.
[17] G.N. George, C.M. Colangelo, J. Dong, R.A. Scott, S.V. Khangulov, V.N. Gladyshev, T.C. Stadtman, J. Am. Chem. Soc. 120 (1998) 1267.
[18] J. Heider, A. Bock, Adv. Microb. Physiol. 35 (1993) 71.
[19] M.J. Axley, A. Bock, T.C. Stadtman, Proc. Natl. Acad. Sci. U. S. A. 88 (1991) 8450.
[20] M.J. Axley, D.A. Grahame, J. Biol. Chem. 266 (1991) 13731.
[21] M. Jormakka, S. Tornroth, B. Byrne, S. Iwata, Science 295 (2002) 1863.
[22] M. Jormakka, S. Tornroth, J. Abramson, B. Byrne, S. Iwata, Acta Crystallogr. D Biol. Crystallogr. 58 (2002) 160.
[23] C.C. Page, C.C. Moser, X.X. Chen, P.L. Dutton, Nature 402 (1999) 47.
[24] A. Volbeda, M.H. Charon, C. Piras, E.C. Hatchikian, M. Frey, J.C. Fontecilla-Camps, Nature 373 (1995) 580.
[25] T.M. Iverson, C. Luna-Chavez, G. Cecchini, D.C. Rees, Science 284 (1999) 1961.

[26] C.R. Lancaster, A. Kroger, M. Auer, H. Michel, Nature 402 (1999) 377.
[27] R.G. Efremov, R. Baradaran, L.A. Sazanov, Nature 465 (2010) 441.
[28] L.A. Sazanov, P. Hinchliffe, Science 311 (2006) 1430.
[29] C. Hunte, V. Zickermann, U. Brandt, Science 329 (2010) 448.
[30] D. Richardson, G. Sawers, Science 295 (2002) 1842.
[31] M.J. Almendra, C.D. Brondino, O. Gavel, A.S. Pereira, P. Tavares, S. Bursakov, R. Duarte, J. Caldeira, J.J. Moura, I. Moura, Biochemistry 38 (1999) 16366.
[32] H. Raaijmakers, S. Macieira, J.M. Dias, S. Teixeira, S. Bursakov, R. Huber, J.J. Moura, I. Moura, M.J. Romao, Structure 10 (2002) 1261.
[33] H. Raaijmakers, S. Teixeira, J.M. Dias, M.J. Almendra, C.D. Brondino, I. Moura, J.J. Moura, M.J. Romao, J. Biol. Inorg. Chem. 6 (2001) 398.
[34] M. Rudolf, P.M. Kroneck, Met. Ions Biol. Syst. 43 (2005) 75.
[35] J.M. Dias, M.E. Than, A. Humm, R. Huber, G.P. Bourenkov, H.D. Bartunik, S. Bursakov, J. Calvete, J. Caldeira, C. Carneiro, J.J. Moura, I. Moura, M.J. Romao, Structure 7 (1999) 65.
[36] S. Najmudin, P.J. Gonzalez, J. Trincao, C. Coelho, A. Mukhopadhyay, N.M. Cerqueira, C.C. Romao, I. Moura, J.J. Moura, C.D. Brondino, M.J. Romao, J. Biol. Inorg. Chem. 13 (2008) 737.
[37] W. Kaim, B. Schwederski, Coord. Chem. Rev. 254 (2010) 1580.
[38] M. Cerqueira, P.J. Gonzalez, C.D. Brondino, M.J. Romao, C.C. Romao, I. Moura, J.J. Moura, J. Comput. Chem 30 (2009) 2466.
[39] P. Arnoux, M. Sabaty, J. Alric, B. Frangioni, B. Guigliarelli, J.M. Adriano, D. Pignol, Nat. Struct. Biol. 10 (2003) 928.
[40] M.G. Bertero, R.A. Rothery, M. Palak, C. Hou, D. Lim, F. Blasco, J.H. Weiner, N.C. Strynadka, Nat. Struct. Biol. 10 (2003) 681.
[41] R.A. Rothery, M.G. Bertero, T. Spreter, N. Bouromand, N.C. Strynadka, J.H. Weiner, J. Biol. Chem. 285 (2010) 8801.
[42] S.P. Kramer, J.L. Johnson, A.A. Ribeiro, D.S. Millington, K.V. Rajagopalan, J. Biol. Chem. 262 (1987) 16357.
[43] M. Jormakka, D. Richardson, B. Byrne, S. Iwata, Structure 12 (2004) 95.
[44] M. Jormakka, K. Yokoyama, T. Yano, M. Tamakoshi, S. Akimoto, T. Shimamura, P. Curmi, S. Iwata, Nat. Struct. Mol. Biol. 15 (2008) 730.
[45] O. Kniemeyer, J. Heider, J. Biol. Chem. 276 (2001) 21381.
[46] D.P. Kloer, C. Hagel, J. Heider, G.E. Schulz, Structure 14 (2006) 1377.
[47] M. Szaleniec, C. Hagel, M. Menke, P. Nowak, M. Witko, J. Heider, Biochemistry 46 (2007) 7637.
[48] M. Szaleniec, T. Borowski, K. Schuhle, M. Witko, J. Heider, J. Am. Chem. Soc. 132 (2010) 6014.
[49] F. Schneider, J. Lowe, R. Huber, H. Schindelin, C. Kisker, J. Knablein, J. Mol. Biol. 263 (1996) 53.
[50] A.S. McAlpine, A.G. McEwan, A.L. Shaw, S. Bailey, J. Biol. Inorg. Chem. 2 (1997) 690.
[51] H.K. Li, C. Temple, K.V. Rajagopalan, H. Schindelin, J. Am. Chem. Soc. 122 (2000) 7673.
[52] G.N. George, J. Hilton, K.V. Rajagopalan, J. Am. Chem. Soc. 118 (1996) 1113.
[53] G.N. George, J. Hilton, C. Temple, R.C. Prince, K.V. Rajagopalan, J. Am. Chem. Soc. 121 (1999) 1256.
[54] R.C. Bray, B. Adams, A.T. Smith, B. Bennett, S. Bailey, Biochemistry 39 (2000) 11258.
[55] R.C. Bray, B. Adams, A.T. Smith, R.L. Richards, D.J. Lowe, S. Bailey, Biochemistry 40 (2001) 9810.
[56] A.S. McAlpine, A.G. McEwan, S. Bailey, J. Mol. Biol. 275 (1998) 613.
[57] L.J. Stewart, S. Bailey, B. Bennett, J.M. Charnock, C.D. Garner, A.S. McAlpine, J. Mol. Biol. 299 (2000) 593.
[58] A. Messerschmidt, H. Niessen, D. Abt, O. Einsle, B. Schink, P.M. Kroneck, Proc. Natl. Acad. Sci. U. S. A. 101 (2004) 11571.
[59] C. Paizs, U. Bartlewski-Hof, J. Retey, Chemistry 13 (2007) 2805.
[60] G.B. Seiffert, G.M. Ullmann, A. Messerschmidt, B. Schink, P.M. Kroneck, O. Einsle, Proc. Natl. Acad. Sci. U. S. A. 104 (2007) 3073.
[61] M.A. Vincent, I.H. Hillier, G. Periyasamy, N.A. Burton, Dalton Trans. 39 (2010) 3816.
[62] G.L. Anderson, J. Williams, R. Hille, J. Biol. Chem. 267 (1992) 23674.
[63] P.J. Ellis, T. Conrads, R. Hille, P. Kuhn, Structure 9 (2001) 125.
[64] R. Hille, Arch. Biochem. Biophys. 433 (2005) 107.
[65] C.D. Brondino, M.J. Romao, I. Moura, J.J. Moura, Curr. Opin. Chem. Biol. 10 (2006) 109.
[66] M.P. Coughlan, K.V. Rajagopalan, P. Handler, J. Biol. Chem. 244 (1969) 2658.
[67] M.P. Coughlan, J.L. Johnson, K.V. Rajagopalan, J. Biol. Chem. 255 (1980) 2694.
[68] V. Massey, D. Edmondson, J. Biol. Chem. 245 (1970) 6595.
[69] R.C. Wahl, K.V. Rajagopalan, J. Biol. Chem. 257 (1982) 1354.
[70] C.J. Doonan, N.D. Rubie, K. Peariso, H.H. Harris, S.Z. Knottenbelt, G.N. George, C.G. Young, M.L. Kirk, J. Am. Chem. Soc. 130 (2008) 55.
[71] T. Santos-Silva, F. Ferroni, A. Thapper, J. Marangon, P.J. Gonzalez, A.C. Rizzi, I. Moura, J.J. Moura, M.J. Romao, C.D. Brondino, J. Am. Chem. Soc. 131 (2009) 7990.
[72] B.T. Eger, K. Okamoto, C. Enroth, M. Sato, T. Nishino, E.F. Pai, Acta Crystallogr. D Biol. Crystallogr. 56 (2000) 1656.
[73] C. Enroth, B.T. Eger, K. Okamoto, T. Nishino, E.F. Pai, Proc. Natl. Acad. Sci. U. S. A. 97 (2000) 10723.
[74] R. Huber, P. Hof, R.O. Duarte, J.J. Moura, I. Moura, M.Y. Liu, J. LeGall, R. Hille, M. Archer, M.J. Romao, Proc. Natl. Acad. Sci. U. S. A. 93 (1996) 8846.
[75] G. Palmer, V. Massey, J. Biol. Chem. 244 (1969) 2614.
[76] R. Hille, W.R. Hagen, W.R. Dunham, J. Biol. Chem. 260 (1985) 10569.
[77] N.G. Leferink, D.P. Heuts, M.W. Fraaije, W.J. van Berkel, Arch. Biochem. Biophys. 474 (2008) 292.
[78] H. Dobbek, L. Gremer, O. Meyer, R. Huber, Proc. Natl. Acad. Sci. U. S. A. 96 (1999) 8884.
[79] Y. Kuwabara, T. Nishino, K. Okamoto, T. Matsumura, B.T. Eger, E.F. Pai, Proc. Natl. Acad. Sci. U. S. A. 100 (2003) 8170.
[80] T. Nishino, K. Okamoto, Y. Kawaguchi, H. Hori, T. Matsumura, B.T. Eger, E.F. Pai, J. Biol. Chem. 280 (2005) 24888.
[81] R. Asai, T. Nishino, T. Matsumura, K. Okamoto, K. Igarashi, E.F. Pai, J. Biochem. 141 (2007) 525.
[82] S. Schumann, M. Saggu, N. Moller, S.D. Anker, F. Lendzian, P. Hildebrandt, S. Leimkuhler, J. Biol. Chem. 283 (2008) 16602.
[83] K. Okamoto, B.T. Eger, T. Nishino, E.F. Pai, Nucleosides Nucleotides Nucleic Acids 27 (2008) 888.
[84] A. Fukunari, K. Okamoto, T. Nishino, B.T. Eger, E.F. Pai, M. Kamezawa, I. Yamada, N. Kato, J. Pharmacol. Exp. Ther. 311 (2004) 519.
[85] K. Okamoto, K. Matsumoto, R. Hille, B.T. Eger, E.F. Pai, T. Nishino, Proc. Natl. Acad. Sci. U. S. A. 101 (2004) 7931.
[86] H. Dobbek, L. Gremer, R. Kiefersauer, R. Huber, O. Meyer, Proc. Natl. Acad. Sci. U. S. A. 99 (2002) 15971.
[87] I. Bonin, B.M. Martins, V. Purvanov, S. Fetzner, R. Huber, H. Dobbek, Structure 12 (2004) 1425.
[88] N. Wagener, A.J. Pierik, A. Ibdah, R. Hille, H. Dobbek, Proc. Natl. Acad. Sci. U. S. A. 106 (2009) 11055.
[89] J.M. Pauff, J. Zhang, C.E. Bell, R. Hille, J. Biol. Chem. 283 (2008) 4818.
[90] U. Dietzel, J. Kuper, J.A. Doebbler, A. Schulte, J.J. Truglio, S. Leimkuhler, C. Kisker, J. Biol. Chem. 284 (2009) 8768.
[91] H. Cao, J.M. Pauff, R. Hille, J. Biol. Chem. 285 (2010).
[92] Y. Yamaguchi, T. Matsumura, K. Ichida, K. Okamoto, T. Nishino, J. Biochem. 141 (2007) 513.
[93] M.J. Romao, M. Archer, I. Moura, J.J. Moura, J. LeGall, R. Engh, M. Schneider, P. Hof, R. Huber, Science 270 (1995) 1170.
[94] J.M. Rebelo, J.M. Dias, R. Huber, J.J. Moura, M.J. Romao, J. Biol. Inorg. Chem. 6 (2001) 791.
[95] S.L. Andrade, C.D. Brondino, M.J. Feio, I. Moura, J.J. Moura, Eur. J. Biochem. 267 (2000) 2054.
[96] D.R. Boer, A. Thapper, C.D. Brondino, M.J. Romao, J.J. Moura, J. Am. Chem. Soc. 126 (2004) 8614.
[97] A. Thapper, D.R. Boer, C.D. Brondino, J.J. Moura, M.J. Romao, J. Biol. Inorg. Chem. 12 (2007) 353.
[98] S. Gutteridge, R.C. Bray, Biochem. J. 189 (1980) 615.
[99] B.D. Howes, R.C. Bray, R.L. Richards, N.A. Turner, B. Bennett, D.J. Lowe, Biochemistry 35 (1996) 1432.
[100] M. Shanmugam, B. Zhang, R.L. McNaughton, R.A. Kinney, R. Hille, B.M. Hoffman, J. Am. Chem. Soc. 132 (2010) 14015.
[101] R. Hille, Met. Ions. Life. Sci. 6 (2009) 395.
[102] J. Rebelo, S. Macieira, J.M. Dias, R. Huber, C.S. Ascenso, F. Rusnak, J.J. Moura, I. Moura, M.J. Romao, J. Mol. Biol. 297 (2000) 135.
[103] M. Boll, Biochim. Biophys. Acta 1707 (2005) 34.
[104] M. Boll, G. Fuchs, Biol. Chem. 386 (2005) 989.
[105] M. Unciuleac, E. Warkentin, C.C. Page, M. Boll, U. Ermler, Structure 12 (2004) 2249.
[106] J. Johannes, M.C. Unciuleac, T. Friedrich, E. Warkentin, U. Ermler, M. Boll, Biochemistry 47 (2008) 4964.
[107] R. Bauder, B. Tshisuaka, F. Lingens, Biol. Chem. Hoppe Seyler 371 (1990) 1137.
[108] J.S. Holcenberg, E.R. Stadtman, J. Biol. Chem. 244 (1969) 1194.
[109] D. Imhoff, J.R. Andreesen, FEMS Microbiol. Lett. 5 (1979) 155.
[110] J.R. Andreesen, R. Wagner, D. Imhoff, P. Durre, Hoppe-Seylers Z. Physiol. Chem. 360 (1979) 1123.
[111] G.L. Dilworth, Arch. Biochem. Biophys. 219 (1982) 30.
[112] V.N. Gladyshev, S.V. Khangulov, T.C. Stadtman, Proc. Natl. Acad. Sci. U. S. A. 91 (1994) 232.
[113] T. Schrader, A. Rienhofer, J.R. Andreesen, Eur. J. Biochem. 264 (1999) 862.
[114] R. Wagner, J.R. Andreesen, Arch. Microbiol. 121 (1979) 255.
[115] W.T. Self, T.C. Stadtman, Proc. Natl. Acad. Sci. U. S. A. 97 (2000) 7208.
[116] S. Metz, W. Thiel, J. Phys. Chem. B 114 (2010) 1506.
[117] J.H. Jeoung, H. Dobbek, Science 318 (2007) 1461.
[118] C. Gourlay, D.J. Nielsen, J.M. White, S.Z. Knottenbelt, M.L. Kirk, C.G. Young, J. Am. Chem. Soc. 128 (2006) 2164.
[119] M. Resch, H. Dobbek, O. Meyer, J. Biol. Inorg. Chem. 10 (2005) 518.
[120] P. Hanzelmann, H. Dobbek, L. Gremer, R. Huber, O. Meyer, J. Mol. Biol. 301 (2000) 1221.
[121] C. Kisker, H. Schindelin, A. Pacheco, W.A. Wehbi, R.M. Garrett, K.V. Rajagopalan, J.H. Enemark, D.C. Rees, Cell 91 (1997) 973.
[122] C. Feng, R.V. Kedia, J.T. Hazzard, J.K. Hurley, G. Tollin, J.H. Enemark, Biochemistry 41 (2002) 5816.
[123] A.K. Rappe, W.A. Goddard, Nature 285 (1980) 311.
[124] E. Karakas, H.L. Wilson, T.N. Graf, S. Xiang, S. Jaramillo-Busquets, K.V. Rajagopalan, C. Kisker, J. Biol. Chem. 280 (2005) 33506.
[125] N. Schrader, K. Fischer, K. Theis, R.R. Mendel, G. Schwarz, C. Kisker, Structure 11 (2003) 1251.
[126] U. Kappler, S. Bailey, J. Biol. Chem. 280 (2005) 24999.
[127] C. Feng, H.L. Wilson, J.K. Hurley, J.T. Hazzard, G. Tollin, K.V. Rajagopalan, J.H. Enemark, Biochemistry 42 (2003) 12235.
[128] U. Kappler, S. Bailey, C. Feng, M.J. Honeychurch, G.R. Hanson, P.V. Bernhardt, G. Tollin, J.H. Enemark, Biochemistry 45 (2006) 9696.
[129] S. Bailey, T. Rapson, K. Johnson-Winters, A.V. Astashkin, J.H. Enemark, U. Kappler, J. Biol. Chem. 284 (2009) 2053.

[130] K. Fischer, G.G. Barbier, H.J. Hecht, R.R. Mendel, W.H. Campbell, G. Schwarz, Plant Cell 17 (2005) 1167.
[131] L. Loschi, S.J. Brokx, T.L. Hills, G. Zhang, M.G. Bertero, A.L. Lovering, J.H. Weiner, N.C. Strynadka, J. Biol. Chem. 279 (2004) 50391.
[132] S.J. Brokx, R.A. Rothery, G. Zhang, D.P. Ng, J.H. Weiner, Biochemistry 44 (2005) 10339.
[133] G.J. Workun, K. Moquin, R.A. Rothery, J.H. Weiner, Microbiol. Mol. Biol. Rev. 72 (2008) 228.
[134] M.K. Chan, S. Mukund, A. Kletzin, M.W. Adams, D.C. Rees, Science 267 (1995) 1463.
[135] Y. Hu, S. Faham, R. Roy, M.W. Adams, D.C. Rees, J. Mol. Biol. 286 (1999) 899.
[136] J.M. Pauff, H. Cao, R. Hille, J. Biol. Chem. 284 (2009) 8760.
[137] J.J. Truglio, K. Theis, S. Leimkuhler, R. Rappa, K.V. Rajagopalan, C. Kisker, Structure 10 (2002) 115.
[138] J.C. Hermann, E. Ghanem, Y. Li, F.M. Raushel, J.J. Irwin, B.K. Shoichet, J. Am. Chem. Soc. 128 (2006) 15882.
[139] J.C. Hermann, R. Marti-Arbona, A.A. Fedorov, E. Fedorov, S.C. Almo, B.K. Shoichet, F.M. Raushel, Nature 448 (2007) 775.
[140] PyMol, The PyMOL Molecular Graphics System, Version 1.2r3pre, Schrödinger, LLC, 2010.